NASA/TM—2000-210206

Slow Crack Growth Behavior and Life/ Reliability Analysis of 96 wt % Alumina at Ambient Temperature With Various Specimen/Loading Configurations

Sung R. Choi, Lynn M. Powers, and Noel N. Nemeth
Glenn Research Center, Cleveland, Ohio

National Aeronautics and
Space Administration

Glenn Research Center

July 2000

Acknowledgments

The authors are thankful to R. Pawlik for the experimental work during the course of this work. This work was sponsored in part by the Ceramic Technology Project, DOE Office of Transportation Technologies, under contract DE-AC05-84OR21400 with Martin Marietta Energy System, Inc.

Available from

NASA Center for Aerospace Information
7121 Standard Drive
Hanover, MD 21076
Price Code: A03

National Technical Information Service
5285 Port Royal Road
Springfield, VA 22100
Price Code: A03

Slow Crack Growth Behavior and Life/Reliability Analysis of 96 wt % Alumina at Ambient Temperature With Various Specimen/Loading Configurations

Sung R. Choi, Lynn M. Powers and Noel N. Nemeth
National Aeronautics and Space Administration
Glenn Research Center
Cleveland, Ohio 44135

SUMMARY

Extensive constant stress-rate testing for 96 wt % alumina was conducted in room-temperature distilled water using four different specimen/loading configurations: rectangular beam test specimens under four-point uniaxial flexure, square plate test specimens in ring-on-ring biaxial flexure, square plate test specimens in ball-on-ring biaxial flexure, and dog-boned tensile test specimens in pure tension. The slow crack growth (SCG) parameter n was almost independent of specimen/loading configurations, in either four-point uniaxial flexure, ring-on-ring biaxial flexure, ball-on-ring biaxial flexure, or pure tension, ranging from $n = 35$ to 47 with an average value of $n = 41.1 \pm 4.5$. The prediction of fatigue strength/reliability based on the four-point uniaxial flexure data by using the CARES/*Life* design code as well as a simple PIA model was in good agreement with both the ring-on-ring biaxial and the ball-on-ring biaxial flexure data. A poor prediction using the PIA model was observed for the dog-boned tensile test specimens, presumably due to different flaw population involved in the tensile test specimens.

INTRODUCTION

Advanced ceramics are candidate materials for structural applications in advanced heat engines and heat recovery systems. The major limitation of these materials in high temperature applications is slow crack growth ('fatigue')-associated failure, where slow crack growth (SCG) of inherent defects or flaws can occur until a critical size for catastrophic failure is reached. Some aluminas have exhibited slow crack growth even at low temperatures including ambient temperature. Therefore, in order to ensure accurate life prediction of ceramic components, it is important to accurately evaluate slow crack growth behavior or SCG parameters of the material with specified loading and temperature conditions.

There are several ways of determining SCG parameters of a ceramic or brittle material. Typically, constant stress-rate (also called "dynamic fatigue"), constant stress ("static fatigue"), or cyclic stress ("cyclic fatigue") testing is conducted with ground specimens with inherent flaws or to precracked fracture mechanics specimens in which the crack velocity measurements are made directly. The SCG parameters required for life prediction/reliability can be determined from appropriate relations between strength and applied stress rate for constant stress-rate testing, and between time-to-failure and applied stress for both constant stress and cyclic stress testing. Because of its simplicity, constant stress-rate testing has been used for several decades and has merit over other methods in some cases. Strength is determined in a routine manner at four to five stress rates by applying constant crosshead speeds (displacement control) or constant loading rates (load control).

Extensive constant stress-rate testing for 96 wt % alumina was conducted in distilled water at ambient temperature to determine slow crack growth behavior of 96 wt % alumina using various specimen/loading configurations. Four different specimen/loading configurations were used: four-point uniaxial flexure with rectangular beam specimens, ring-on-ring biaxial flexure with square plate specimens, ball-on-ring biaxial flexure with square plate specimens, and pure tension with dog-boned, cylindrical specimens. A special emphasis on experiments was placed in the development of pure tension testing where a series of different testing techniques had to be followed to come up with an assured test methodology. The SCG and reliability parameters obtained from four-point uniaxial flexure with rectangular beam specimens (ref. 1) were taken as baseline data in predicting the SCG behavior of other specimen/loading configurations. The life prediction/reliability was made using both the CARES/*Life* computer code developed at the NASA Glenn (ref. 2) and the simple analytical PIA (principle of independent action) model (refs. 3 and 4)

EXPERIMENTAL PROCEDURES

Material

The material used in this study was isopressed, 96 wt % alumina, fabricated by General Electrical Ceramic (Laurens, SC), designated as Alsimag 614. The major physical and mechanical properties of the material are summarized in table I. The material had been used for the determination of strength and slow crack growth behaviors at ambient temperature (refs. 1 and 5) before this work was completed (in 1996). The microstructure of the material, typified as a somewhat bimodal grain structure, is shown in figure 1. This material containing glassy phases has exhibited a moderate SCG in room-temperature distilled water with a SCG parameter of $n \approx 40$ to 50 (refs. 1 and 5) so that it was considered as an ideal material to model SCG behavior under different specimen/loading configurations.

TABLE I.—BASIC MECHANICAL AND PHYSICAL PROPERTIES OF 96 WT % ALUMINA AT AMBIENT TEMPERATURE

Density,[a] g/cm^3	Young's modulus,[b] GPa	Hardness,[c] GPa	Poisson's ratio[b]	Fracture toughness,[d] MPa$\sqrt{m}$	Inert strength,[e] MPa
3.65	302	10.0	0.24	3.1 ± 0.2	295.4 ± 17.0

[a]By bulk mass method.
[b]By impulse excitation method with disks (ASTM C1259).
[c]By Vickers hardness method (ASTM C1327).
[d]By SEPB method (ASTM C 1421)
[e]By four-point flexure (20/40 mm spans) (ASTM C1611).

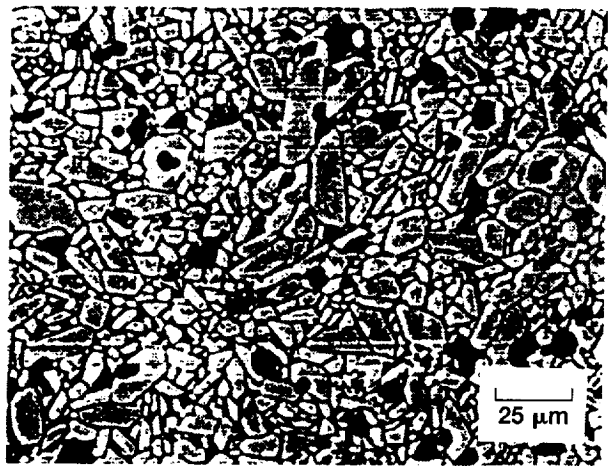

Figure 1.—Microstructure of 96 wt% alumina used in this study.

Constant Stress-Rate Testing

Constant stress-rate (also called "dynamic fatigue") testing employs a series of stress rates, four to five, to determine the corresponding fracture strengths. The susceptibility to slow crack growth of a material can be measured from a degree of strength degradation with respect to applied stress rate. The strength as a function of stress rate subjected to constant stress-rate testing can be expressed as follows (ref. 6):

$$\sigma_f = D[\dot{\sigma}]^{\frac{1}{n+1}} \tag{1}$$

where σ_f is the fracture strength, $\dot{\sigma}$ is the applied stress rate, D and n are the SCG parameters. The above equation can be derived based on the fundamental assumption that SCG of ceramics and glass is governed by the power-law crack velocity (ref. 7)

$$v = \frac{da}{dt} = A\left[\frac{K_I}{K_{IC}}\right]^n \tag{2}$$

where v is the crack velocity, a the crack size, t the time, K_I the mode I stress intensity factor, K_{IC} the fracture toughness of a material, and A and n are the SCG parameters. The SCG parameters n and D in equation (1) can be determined from the slope and the intercept of the data (curve), respectively, via a linear regression analysis when log (fracture strength) was plotted as a function of log (stress rate). There are two widely utilized methods in estimating the SCG parameters n and D, which are individual data method and arithmetic mean method. The individual data method uses the individual strength (not-averaged) with each individual stress rate (not-averaged) in the linear regression analysis; while the arithmetic mean method uses the arithmetic mean strength with mean stress rates. It has been shown that little difference was found in the values of n and D between the two methods for the case of Weibull modulus $m \geq 10$ (ref. 8). The parameter A can be estimated from D with an appropriate relation (ref. 9). The simplicity of the constant stress-rate test method had prompted an effort to establish an ASTM standard within the C28 Advanced Ceramics Committee to determine SCG parameters of advanced ceramics (ref. 10). A full consensus Test Method C1368 has been developed in 1997 (ref. 11). In Test Method C 1368, the individual data method is recommended in determining SCG parameters n and D. Detailed test procedure will be described below. The overall test specimen/loading configurations used in this study are summarized in figure 2.

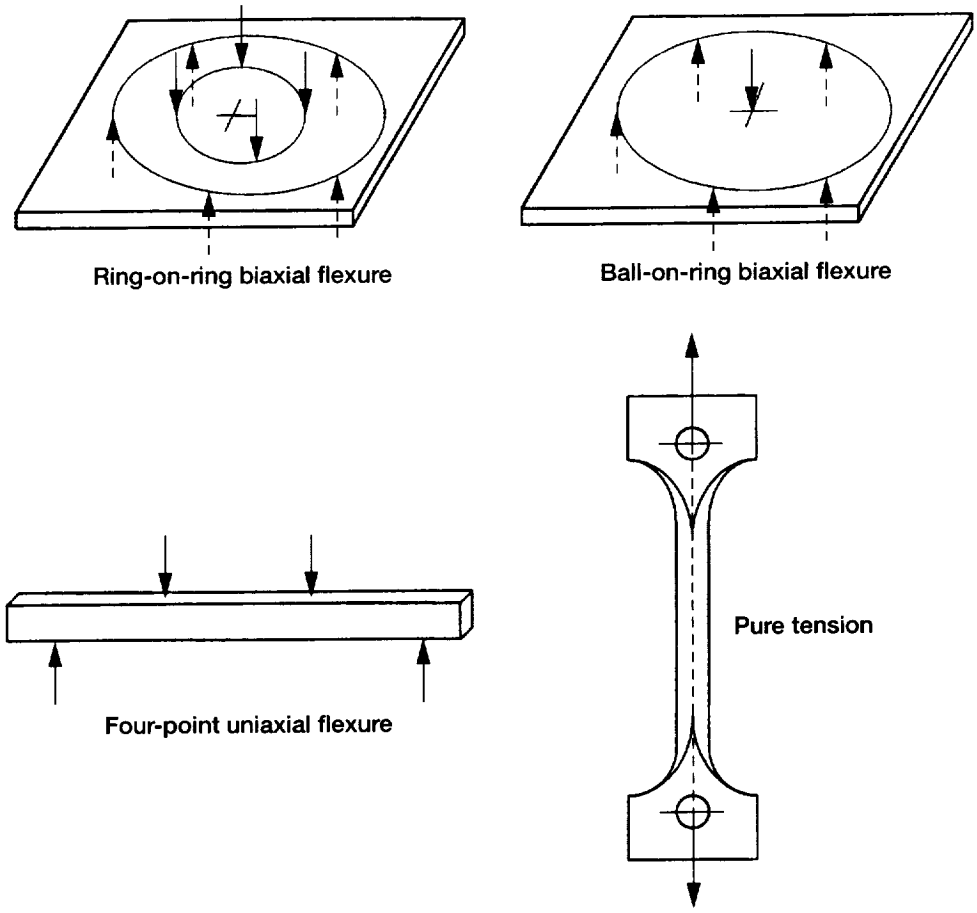

Figure 2.—Test specimen/loading configurations used in this study; Ring-on-ring biaxial flexure, ball-on-ring biaxial flexure, four-point uniaxial flexure, and pure tension.

Four-point uniaxial flexure with rectangular beam specimens.—Constant stress-rate testing in four-point uniaxial flexure was carried out previously (refs. 1 and 5). The test specimens were cut from a billet such that the nominal dimensions of rectangular beam test specimens were 3 by 4 by 50 mm, respectively, in width, thickness and length (Type B, ASTM C 1161). After machining, all the test specimens were annealed in air at 1200 °C for 1 hr to remove or minimize any spurious residual stress and machining damage. Each test specimen was tested in room-temperature distilled water using a stainless steel, four-point flexure fixture with 20 mm-inner and 40 mm-outer spans in accordance with ASTM C 1368. Six different stress rates ranging from 0.0333 to 3333 MP/s were applied by using an electromechanical test frame (Model 8562, Instron, Canton, MA) in load control. A total of ten specimens were used at each stress rate. Inert strength was also determined in silicon oil (704 Diffusion Pump Fluid, Dow Corning, Midland, MI) at a fast stress rate of 33.33 MPa/s with a total of 20 test specimens.

Ring-on-ring biaxial flexure with square plate specimens.—The nominal dimensions of square plate test specimens were 2 by 25 by 25 mm, respectively, in thickness and two sides. The test specimens were annealed at 1200 °C for 1 hr to eliminate or minimize any residual stress and damage associated with machining. Each test specimen was tested in room-temperature distilled water with a ring-on-ring biaxial test fixture with 5.625 mm-loading ring and 10.36 mm-support ring radii. The lower, support-ring fixture consisted of 6 stainless steel balls (9.521 mm diam with a hardness of 60 Rockwell C) placed peripherally on a stainless steel bearing race. A copper ring with a 5.625 mm diameter was used as an upper, loading ring. Four different stress rates ranging from 0.0333 to 2560 MPa/s were applied using the electromechanical test frame in load control. A total of five specimens were used at each stress rate. Inert strength was also measured in silicon oil at 33.33 MPa/s using a total of six specimens. Each test specimen was placed accurately in the test fixture using a specially designed aligning tool so that the center of the test specimen corresponded to the center of the test fixture assembly. The fracture strength (σ_f) was calculated using the following equation (ref. 12):

$$\sigma_f = \frac{3P}{4\pi t^2}\left[2(1+\nu)\ln\frac{a}{b} + \frac{(1-\nu)\left(a^2-b^2\right)}{R^2}\right] \tag{3}$$

where P is the fracture load, t is the specimen thickness, ν is Poisson's ratio, a is the support-ring radius, b is the loading-ring radius, and R is the test specimen radius in disk specimen configuration. The equivalent, test specimen radius (R) for square plate specimens was obtained by the suggestion of Vitman and Pukh (ref. 13):

$$R = \frac{h\left(1+\sqrt{2}\right)}{2} = 1.207h \tag{4}$$

where $2h$ is the side length of a square plate.

Ball-on-ring biaxial flexure with square plate specimens.—The dimensions and heat treatment of square-plate test specimens used in ball-on-ring biaxial flexure testing were the same as those used in ring-on-ring biaxial flexure. The test specimens were tested in room-temperature distilled water using the biaxial flexure test fixture that consisted of an upper, 1.03 mm-uniform contact-loading zone radius and a lower, 10.29 mm-support ring radius. The upper loading fixture with a uniform contact loading zone (that was to be in contact with the center region of compression side of test specimens) was made with a hardened steel ball with its small portion flattened by grinding. The radius of the small flattened, uniform contact loading zone was 1.03 mm. A thrust ball bearing assembly was used for the lower, support-ring fixture. The range and the number of applied stress rates employed in this ball-on-ring biaxial testing were the same as those used in the ring-on-ring biaxial testing. Five specimens were used at each stress rate. The inert strength was determined in silicon oil at 33.33 MPa/s with a total of 4 specimens. As used in the ring-on-ring biaxial flexure testing, a special aligning tool was used to position accurately each test specimen relative to the test fixture assembly. The fracture strength was calculated using the following equation (ref. 12):

$$\sigma_f = \frac{3P(1+\nu)}{4\pi t^2}\left[1 + 2\ln\frac{a}{b} + \frac{1-\nu}{1+\nu}\left(1-\frac{b^2}{2a^2}\right)\frac{a^2}{R^2}\right] \tag{5}$$

where b is the radius of the uniform contact loading zone, and other terms are the same as those defined in equation (3).

Pure tension with dog-boned cylindrical specimens.—The dog-boned, tensile test specimens with round cross-section were cut from the billet. The nominal diameter and the gage length of test specimens were 3 and 20.7 mm, respectively. A drawing of the test specimen is shown in figure 3. Each pin-loading hole was tapered toward the center to improve alignment (ref. 14). The geometry and configuration of the test specimens were similar to those of the NCX 34 silicon nitride tensile specimens previously used for elevated-temperature constant stress ("static fatigue") testing (ref. 15). However, the cross-sections were different. The square cross-section was used for the NCX 34 silicon nitride tensile test specimens; whereas, the round cross-section was used for the 96 wt % alumina test specimens, to minimize or eliminate possible stress concentration frequently occurring at the edges of the square cross-section specimens due to undesirable bending.

It was observed that the tensile test specimens were poorly ground with visible undercuts, chatter marks and/or spirals in the gage sections so that elaborate polishing with SiC papers had to be done to smooth the gage section and to reduce the undercut of each test specimen. The test specimens, after polishing, were then annealed in air at 1200 °C for 1 hr. Several different time-consuming trials were made to achieve an optimum loading configuration for the test specimens with a minimum error, as follows:

Wire-rope loading system: Each lower or upper set of this loading system consisted of a 4.76 mm (3/16 in.)-diameter steel wire rope (with a length of 9 in.) attached at each end with a stainless steel straight-pull end, and a stainless steel specimen grip with a loading pin hole. The test specimen was loaded through the upper and lower loading pins attached to the specimen grips. Because of inherent warping (or twist) of the wire ropes, a rotational displacement was induced to the test specimen during loading. This loading system resulted in a bending strain of

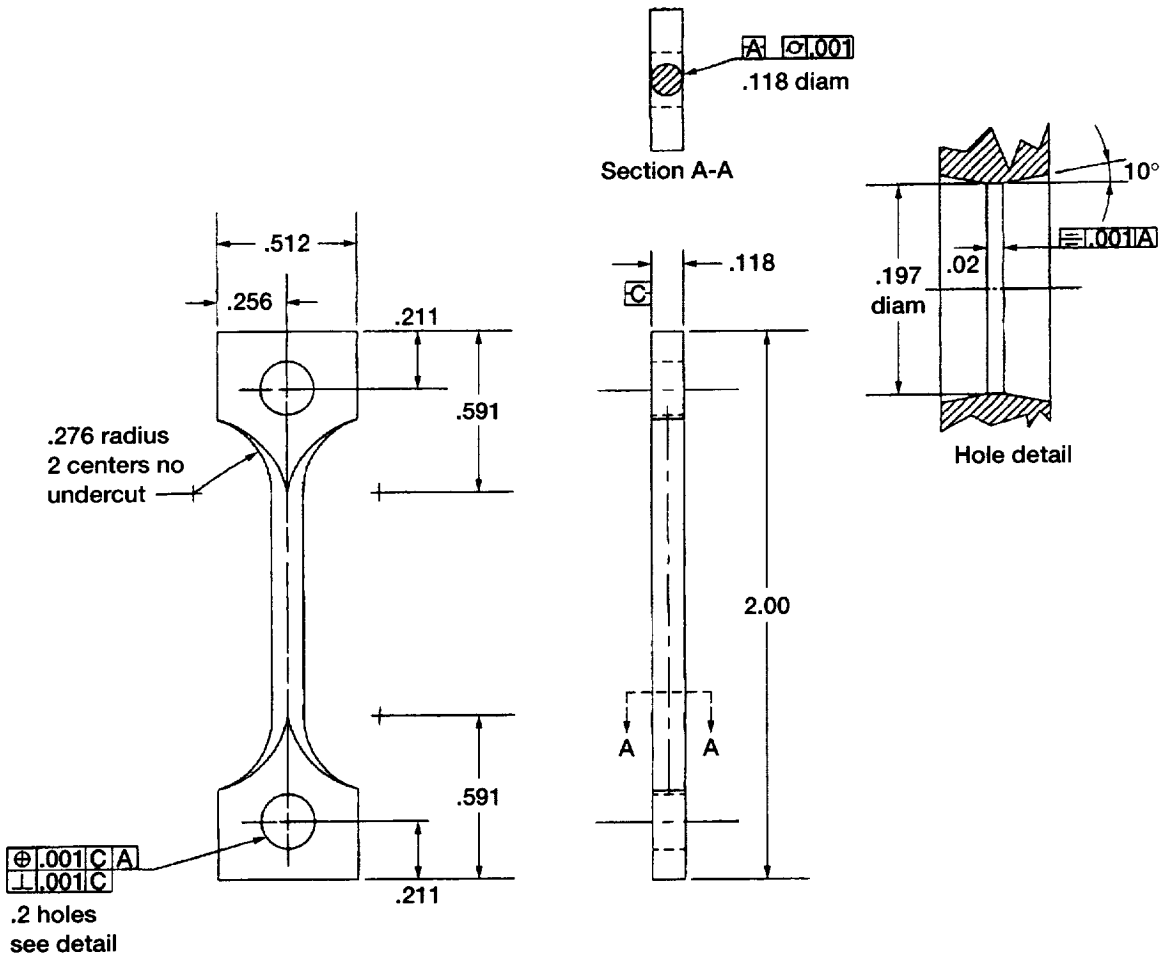

Figure 3.—Schematics of a dog-boned, cylindrical tensile test specimen. Units are in inches.

~11 percent at a tensile load close to failure. The strain was measured with strain gages attached to the gage section of a reference test specimen.

Swivel wire-rope loading system: This was basically the same as the "wire-rope loading system" with the exception of thrust ball bearings installed at the end of each rope to accommodate the rotational displacement of the wire rope. This system, however, did not meet the acceptable alignment level, bending strain <7 percent.

Chain-link loading system: The steel wire rope was replaced with a steel link chain (link dimensions 1.5×1 in. with 1/4 in. diam) with a length of 9.5 in. This setup resulted in better alignment (about 9 percent bending) than the "wire-rope loading system" but not as good as the "swivel wire-rope loading system."

Fixed single-pin loading system: This grip system consisted of the upper and lower grips with a single pin hole for each grip (as used for the wire rope and chain link loading systems), rigidly and directly mounted to the test frame, as shown in figure 4. Alignment of test specimen was optimized using a standard alignment fixture equipped on the test frame. The resulting bending was found to be 2.3 to 14.8 percent depending on the test-specimen orientation in the grips. Because of its simplicity and alignment satisfaction, this system was chosen as a potential loading system and its workability was checked by conducting actual constant stress-rate testing as follow.

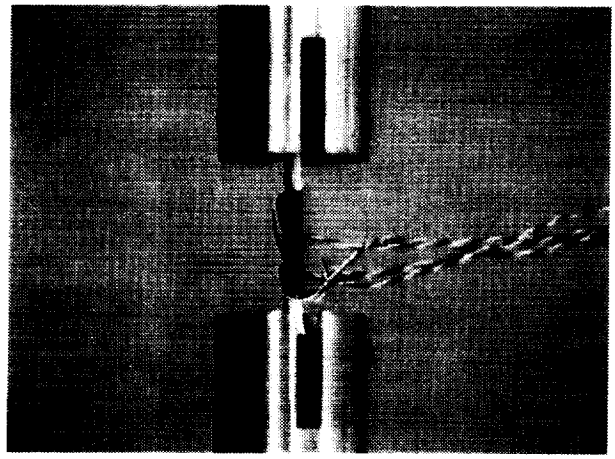

Figure 4.—A dog-boned cylindrical tensile test specimen attached to fixture grips in fixed single-pin loading system.

Constant stress-rate testing was carried out at a lower stress rate of 0.0333 MPa/s with each test specimen immersed in RT distilled water via a plastic container. The first ten specimens, however, failed at the loading-pin holes. Hence, the following attempts were made to determine and/or remedy the problem associated with the pin-hole failure.

i. The heads of each test specimen including pin holes were coated with polyurethane to protect against failure due to slow crack growth accelerated with water.
ii. Similarly, the heads of test specimens were coated with grease.
iii. The loading-pin holes were polished with diamond compound to remove sharp edges and damage due to machining, thus to minimize stress concentration.
iv. The test specimens were annealed with longer annealing time to ensure more crack healing, with 40 hr at 1200 °C.

However, the above attempts combined did not solve the pin-hole failure problem. This prompted the use of strain gages near and inside the pin hole to examine if there might be a possible stress concentration. The stress, parallel in direction to the gage-section tensile stress, was determined at the location close to the pin hole, which lied on the horizontal centerline of the pin hole. The resulting stress was not comparable with that in the gage section. The stress inside the pin hole was estimated from the strain gages placed on the wall of the pin hole, positioned at the

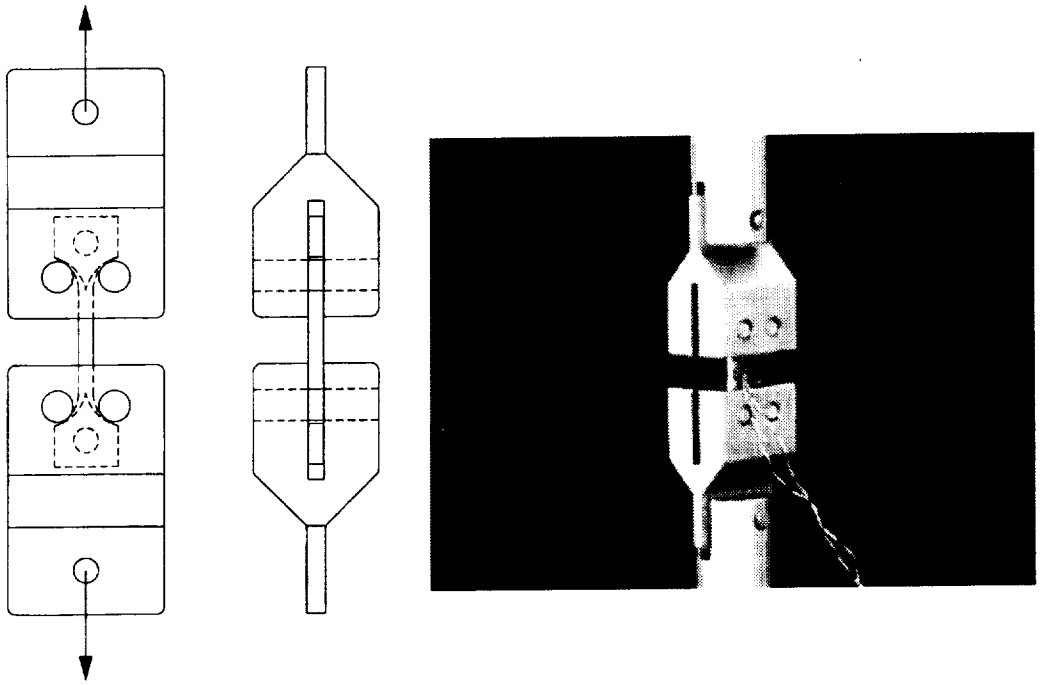

Figure 5.—Schematic of fixed double-pin loading system.

right angle from the vertical centerline of the hole. The tangential stress inside the pin hole was found to be almost twice that of the gage section. This undesirable stress concentration occurring inside the pin hole led to a new fixture design with a double-pin loading system.

Fixed double-pin loading system: This double-pin test fixture has been used previously in tension testing for ceramics (ref. 16). Instead of using single pin-loading (through the pin hole of the test specimen), the test specimen in this fixture was loaded through its shoulders by two loading pins. The details of the fixed double-pin loading system are shown in figure 5. Bending strain was between 0 and 9 percent depending on the specimen orientation and was able to be adjusted within an acceptable level of <7 percent. However, several test specimens failed from the pin/specimen contact regions, associated with Hertzian contact damage. This problem was easily remedied by inserting thin copper shims (0.05 mm thick) between the test-specimen shoulders and the loading pins. The fixed double-pin loading fixture thus modified was utilized throughout the tension testing.

Constant stress-rate tension testing using the fixed double-pin loading fixture was conducted with the dog-boned tension test specimens in room-temperature distilled water using the electromechanical test frame in load-control. Four different stress rates ranging from 0.0333 to 2700 MPa/s were employed. A total of five specimens were used at each stress rate. The inert strength was also determined at 33.33 MPa/s in silicon oil with five test specimens. Figure 6 shows a summary of different modes of failure associated with the test fixtures and the machining conditions of test specimens. The figure includes the pin-hole failure occurring due to stress concentration in the fixed single-pin loading fixture; the shoulder-region failure due to Hertzian contact damage in the fixed double-pin loading fixture; the transition-region failure due to inappropriate machining in the fixed double-pin loading fixture; and the desirable, normal gage-section failure in the fixed double-pin loading fixture

Fractographic Analysis

Some limited fractographic analysis was made to determine the source of failure origin, crack branching length and/or fracture mirror size, if possible. Crack branching lengths for the biaxial flexure test specimens were evaluated by an optical microscope (Olympus, SZH, Japan) in conjunction with a displacement measuring equipment (Boeckler, AZ, Germany). Fracture mirror sizes for the four-point uniaxial flexure test specimens were also determined using the same measuring system. The crack branching constant or fracture mirror constant is related to fracture strength as a function of crack branching length or fracture mirror size as follows (ref. 17):

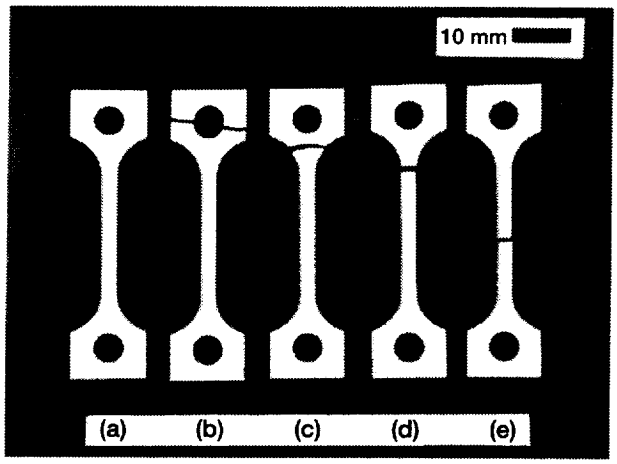

Figure 6.—Summary of different modes of failure for tensile test specimens: (a) Original (untested) test specimen; (b) Pin-hole failure in the fixed single-pin loading system; (c) Shoulder-region failure in the fixed double-pin loading system; (d) Transition-region failure; (e) Normal, gage-section failure in the fixed double-pin loading system.

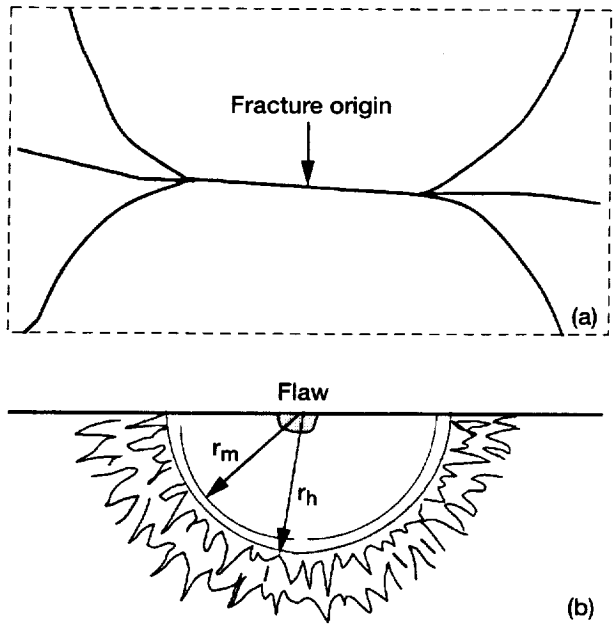

Figure 7.—Schematic of (a) branched cracks and (b) fracture mirror region developed in fracture surface.

$$\sigma_f r^{1/2} = A \tag{6}$$

where r is the crack branching length (radius) or fracture mirror size (radius) in units of meter, as defined in figure 7, and A is the crack branching constant or fracture mirror constant in units of $MPa\sqrt{m}$. The crack branching or fracture mirror constant can be obtained from equation (6) using a functional-fit analysis based on a given set of data on strength versus corresponding crack branching length or fracture mirror size.

RESULTS

Four-point uniaxial flexure with rectangular beam test specimens

The results of constant stress-rate testing for the rectangular beam test specimens in four-point uniaxial flexure are shown in figure 8, where log (fracture strength) was plotted against log (applied stress rate) based on equation (1). The decrease in fracture strength with decreasing stress rate, which represents susceptibility to SCG, is evident from the plot. The SCG parameters, estimated based on equation (1) with units of MPa in strength and MPa/s in stress rate, were $n = 47.24 \pm 3.43$ and $\log D = 2.3486 \pm 0.0029$ by the individual data method. The two-parameter Weibull plot of the inert strength determined with a total of 20 test specimens is shown in figure 9, where the failure probability (F) was plotted as a function of fracture strength based on the distribution equation of $\ln\ln(1/(1-F)) = m \ln \sigma_f + I$ with m and I being Weibull modulus and intercept, respectively. Weibull modulus (m) and characteristic strength (σ_θ) were obtained as $m = 20.2$ and $\sigma_\theta = 303.2$ MPa, respectively. A relatively low scatter in strength (typically, coefficients of variation ≤ 5 percent) was observed for most of the strength data, indicating that the test specimens exhibited high Weibull modulus, $m \geq 20$, regardless of test environment, either in distilled water or in silicon oil.

A typical example of fracture surface of a test specimen tested in a fast test rate of 333 MPa/s is shown in figure 10. Although not all the individual test specimens were fractographically examined, it is believed that most of the specimens tested would have failed from surface flaws or surface defects that were directly exposed to a SCG-enhancing environment, water. A summary of SCG parameters estimated by both the individual data and the arith-

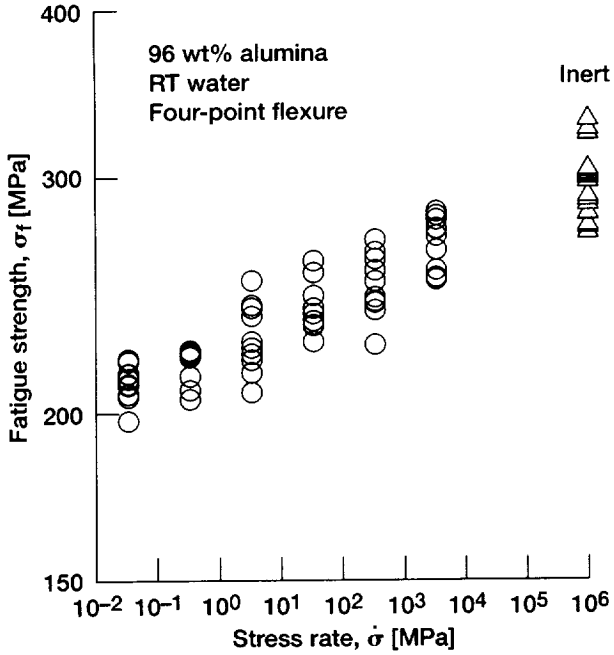

Figure 8.—Results of constant stress-rate testing for alumina in four-point uniaxial flexure in room-temperature distilled water [1]. The inert strength was included for comparison.

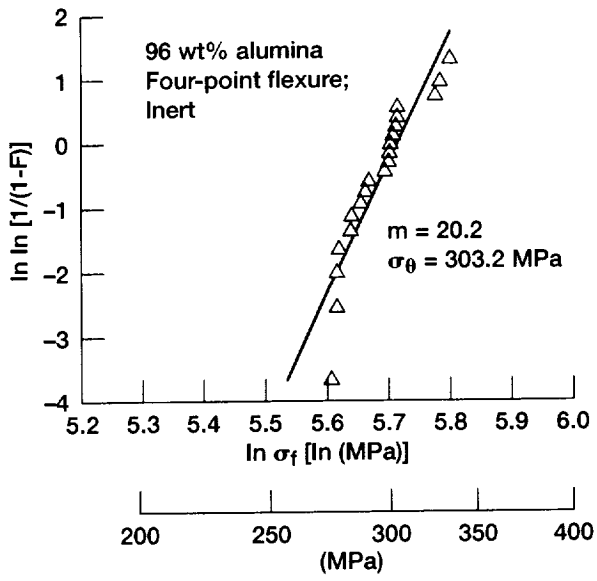

Figure 9.—A Weibull plot of inert strength of alumina in four-point uniaxial flexure in silicon oil at room temperature.

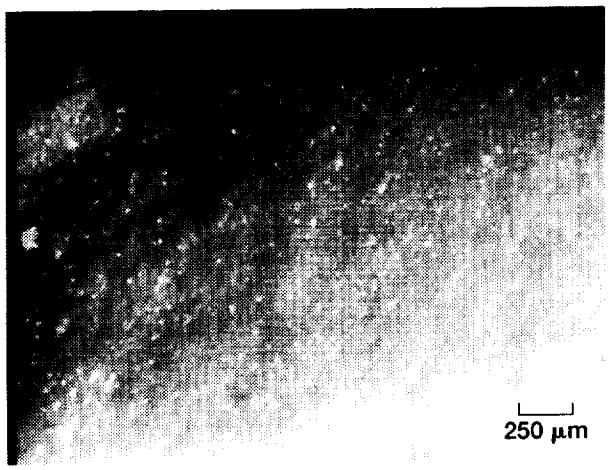

Figure 10.—A typical example of fracture surface of alumina in four-point uniaxial flexure in room-temperature distilled water: $\dot{\sigma}$ = 333 MPa/s; σ_f = 269 MPa.

metic mean methods is shown in table II. As can be seen from the table, the difference in SCG parameters between the two estimation methods was negligible for a given specimen/loading condition, consistent with the previous results for other various advanced ceramics (ref. 8).

Ring-on-Ring Biaxial Flexure With Square Plate Test Specimens

The results of constant stress-rate testing in ring-on-ring biaxial flexure with square plate test specimens are shown in figure 11. The SCG parameters were estimated as $n = 43.34 \pm 4.87$ and $\log D = 2.3187 \pm 0.0050$ by the individual data method (see table II). This value of n is in good agreement with the value of $n = 47.24$ obtained from

TABLE II.—SUMMARY OF SLOW CRACK GROWTH (SCG) PARAMETERS N AND D DETERMINED BY CONSTANT STRESS-RATE TESTING IN ROOM-TEMPERATURE DISTILLED WATER FOR 96 WT % ALUMINA WITH FIVE DIFFERENT SPECIMEN/LOADING CONFIGURATIONS

Specimen/loading configurations	Number of stress rates	Number of test specimens per stress rate	SCG parameters (n and D)			
			By arithmetic mean method		By individual data method	
			n	$Log\ D$	n	$Log\ D$
Four-point flexure (rectangular beam test specimens)	6	10	47.12 [a](3.03)	2.3489 (0.0026)	47.24 (3.43)	2.3486 (0.0029)
Ring-on-ring biaxial flexure (square plate test specimens)	4	5	43.42 (1.40)	2.3191 (0.0014)	43.34 (4.87)	2.3187 (0.0050)
Ball-on-ring biaxial flexure (square plate test specimens)	4	5	35.12 (1.95)	2.3847 (0.0030)	35.53 (3.73)	2.3850 (0.0055)
Pure tension (dog-boned cylindrical test specimens)	4	5	40.10 (2.67)	2.2914 (0.0032)	40.13 (8.29)	2.2898 (0.0099)
Four-point flexure (cylindrical rod test specimens)	2	5	39.72	2.3489	39.37 (7.75)	2.3989 (0.0071)
Average	---	---	41.10 (4.48)	------	41.12 (4.41)	

Note: Units are in MPa for strength and MPa/s for stress rate.

[a]The numbers in parentheses indicate ±1.0 standard deviations.

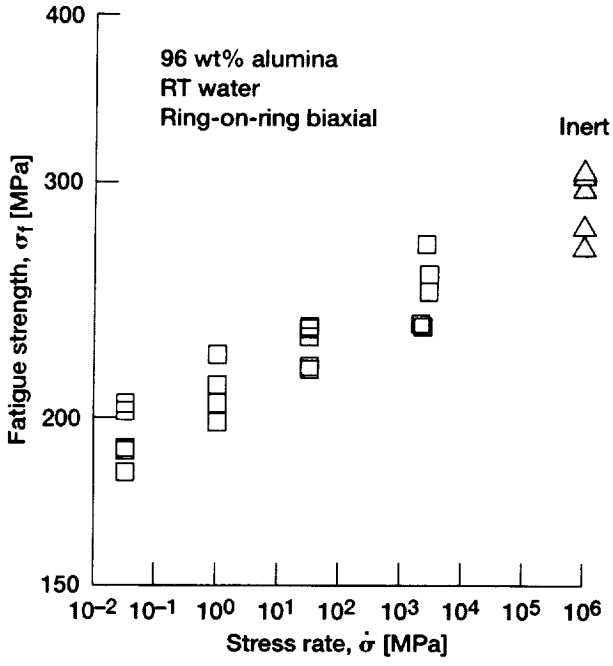

Figure 11.—Results of constant stress-rate testing for alumina square plate specimens in ring-on-ring biaxial flexure in room-temperature distilled water.

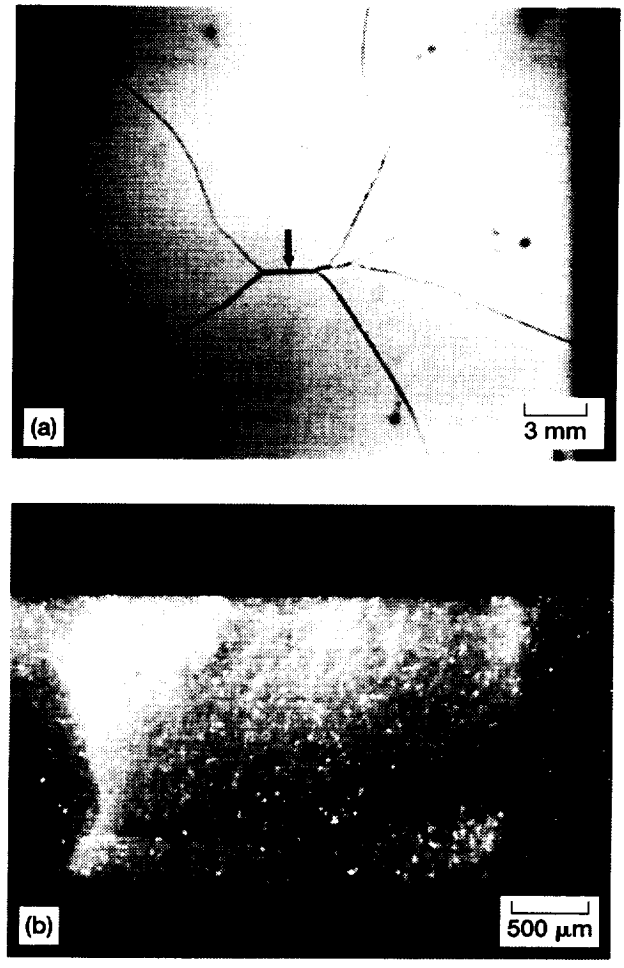

Figure 12.—Typical fracture pattern (a) and fracture surface (b) of an alumina square plate specimen in ring-on-ring biaxial flexure in room-temperature distilled water: $\dot{\sigma}$ = 1.05 MPa/s; σ_f = 223 MPa. The arrow in (a) indicates a flaw origin.

four-point uniaxial flexure loading. All the tested specimens failed within the loading-ring diameter, in which the maximum, biaxial stress state (in both tangential and radial stresses) was attained. Typical examples of crack-branching pattern and fracture surface of a square plate test specimen subjected to a low stress rate of 1.05 MPa/s are shown in figure 12.

Ball-on-Ring Biaxial Flexure With Square Plate Specimens

The test results of constant stress-rate testing in ball-on-ring biaxial flexure with square plate test specimens are depicted in figure 13. The SCG parameters were estimated to be $n = 35.53 \pm 3.73$ and $\log D = 2.3850 \pm 0.0055$, respectively, by the individual data method, as shown in table II. This value of n is 25 and 18 percent lower than the values determined, respectively, in four-point uniaxial flexure and ring-on-ring biaxial flexure. However, considering the appreciable scatter in n that has been commonly observed for many ceramics with the coefficients of variation in n reaching up to 30 percent, such a difference would be regarded less significant. Most of the tested specimens failed at the central loading zone in which the maximum biaxial stresses occurred. Typical examples of crack-branching pattern and fracture surface of a test specimen subjected to a fast stress rate of 2500 MPa/s are shown in figure 14. A reasonably defined mirror region is seen from the fracture surface together with a possible surface-flaw origin.

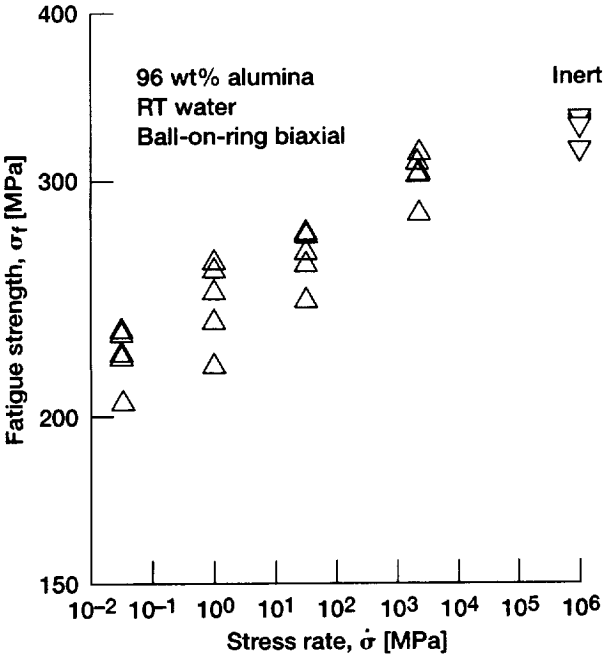

Figure 13.—Results of constant stress-rate testing for alumina square plate specimens in ball-on-ring biaxial flexure in room-temperature distilled water.

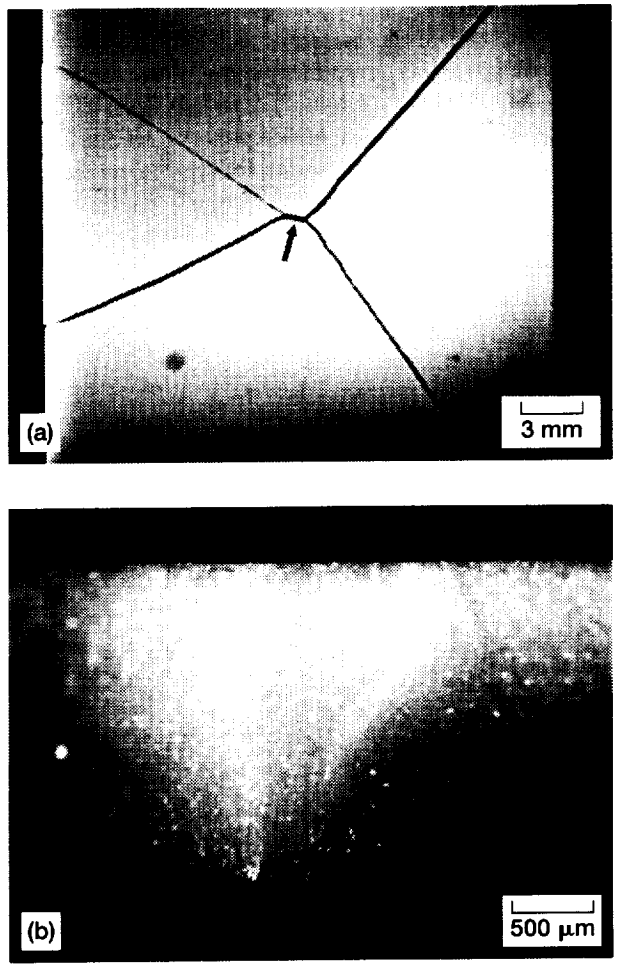

Figure 14.—Typical fracture pattern (a) and fracture surface (b) of an alumina square plate specimen in ball-on-ring biaxial flexure in room-temperature distilled water: $\dot{\sigma}$ = 2500 MPa/s; σ_f = 314 MPa. The arrow in (a) indicates a flaw origin.

Pure Tension With Dog-Boned Tension Specimens

The strength-versus-stress rate results of constant stress-rate tension testing with the dog-boned tension specimens are presented in figure 15. The SCG parameters were found to be $n = 40.13 \pm 8.29$ and $\log D = 2.2898 \pm 0.0099$, as seen in table II. The SCG parameter n is in good agreement particularly with the values obtained from the four-point unaxial flexure and the ring-on-ring biaxial flexure testing. It should be noted, however, that as shown in the figure the strength scatter in pure tension (ranging up to 12 percent in the coefficients of variation) was significantly greater especially at the intermediate stress rates than that (typically <5 percent) observed from either uniaxial or biaxial flexure tests. A typical fracture surface showing a surface flaw-associated failure, due to a machining flaw, is shown in figure 16.

A Summary of Test Results

The results of all the constant stress-rate testing with four different specimen/loading configurations are summarized in figure 17. For clarity, arithmetic mean strengths with error bars were plotted together with the best-fit lines that were determined based on the arithmetic mean strength values. As mentioned above, discrepancy in the SCG parameter n among the four specimen/loading configurations was not appreciable, ranging from $n = 35.5$ to 47.2, with an average value of $n = 41.6 \pm 5.0$. This indicates that the SCG parameter n remained almost constant, irrespective of loading/specimen configurations, confirming again that it is a uniquely defined material/environment constant. Previous results on slow crack growth flexure testing for the same material/environment but with indented four-point beam test specimens showed that the SCG parameter n was 53, 43 and 47, respectively for constant stress-rate ("dynamic fatigue"), constant stress ("static fatigue") and cyclic stress ("cyclic fatigue") testing (ref. 5). Hence, based on the current and previous results it can be concluded that the SCG parameter n of 96 wt % alumina is invariably a material constant for a given environment (water), independent of either specimen/loading configuration, type of slow crack growth (fatigue) testing, or type of flaws (machining flaws, natural flaws, or indent flaws). In fact, the range of SCG parameter n for a variety of aluminas (90 to 99.9 percent) in ambient air or water has been reported as around $n \approx 30$ to 50 (refs. 18 to 22).

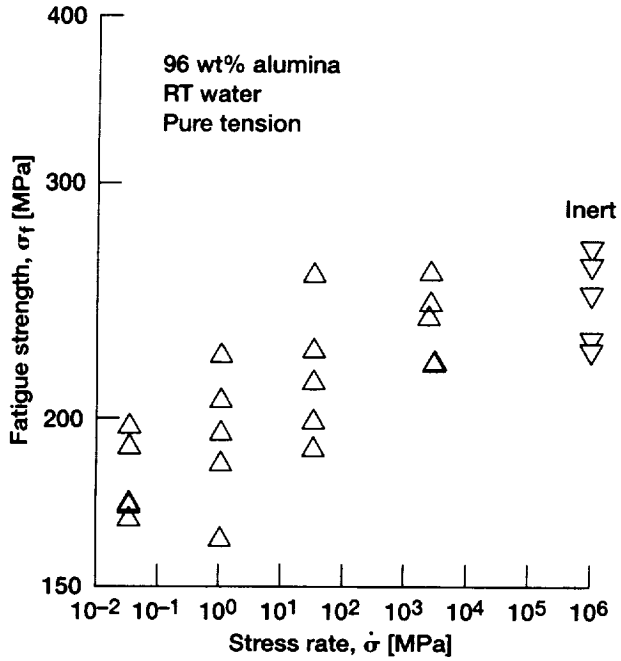

Figure 15.—Results of constant stress-rate testing for dog-boned, alumina cylindrical tensile test specimens in room-temperature distilled water.

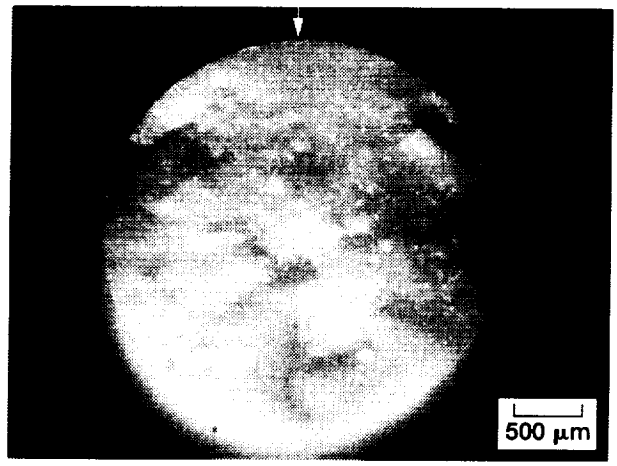

Figure 16.—A typical fracture surface of a dog-boned, alumina cylindrical tensile test specimen in room-temperature distilled water: $\dot{\sigma} = 2500$ MPa/s; $\sigma_f = 219$ MPa. The arrow indicates a flaw origin.

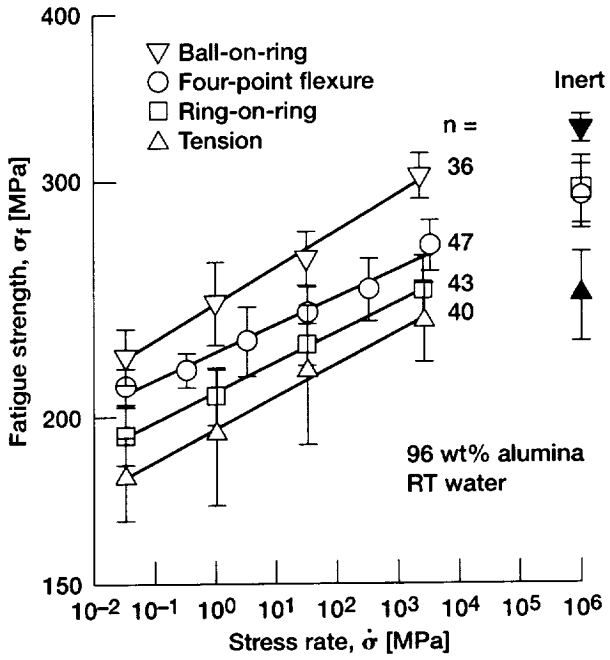

Figure 17.—A summary of constant stress-rate testing for 96 wt% alumina with four different specimen/loading configurations in room-temperature distilled water. The solid lines represent the base-fit lines. The error bars indicate ± 1.0 standard deviation.

The SCG parameter D in equation (1) is expressed as follows (refs. 9 and 11):

$$\log D = \frac{1}{n+1}\log\left[B(n+1)\sigma_i^{n-2}\right] \tag{7}$$

where B is another SCG parameter and σ_i is the inert strength. For a given material/environment, the SCG parameter D is a strong function of inert strength of a material, hence sensitive to the specimen/loading configuration. The SCG parameter D or overall fatigue strength is in increasing order from pure tension (lowest), to ring-on-ring biaxial flexure, to four-point uniaxial flexure, and to ball-on-ring biaxial flexure (highest), as can be seen in table II or figure 17.

Fractographic Analysis

The results on the branched crack measurements from the tested biaxial specimens (inert and fatigue) as well as on the fracture-mirror size measurements from the tested four-point uniaxial flexure specimens (inert and fatigue) are shown in figure 18. For a reasonably accurate data representation in association with the state of stress, crack branching lengths >1.2 mm were not taken as valid data points in biaxial flexure, while fracture mirror sizes >0.9 mm were not taken in four-point unaxial flexure. Fracture mirror was not well-defined with clear demarcation in the fracture surfaces of the tested tension specimens, so it was unable to determine fracture mirror size from those specimens. Based on the results in figure 18 together with equation (6), crack branching and fracture mirror constants can be determined. The crack branching constant was A = 7.24±0.66 and 7.39±0.55 MPa$\sqrt{\text{m}}$, respectively, for ring-on-ring biaxail flexure and ball-on-ring biaxial flexure. The fracture mirror constant for four-point uniaxial flexure was A = 7.63±0.53 MPa$\sqrt{\text{m}}$. A summary of strength versus branched length or mirror size including all the three cases is shown in figure 18(d). As seen in the figure, there was no appreciable difference in the values of A, ranging from A = 7.2 to 7.6 MPa$\sqrt{\text{m}}$, regardless of specimen/loading configuration (either biaxial flexure, uniaxial flexure, or pure tension) and test environment (either water or inert medium). The ratio of crack branching or mirror constant to fracture toughness was A/K_{IC} = 2.33 to 2.66. A relatively large range in A/K_{IC} ratio, ranging from

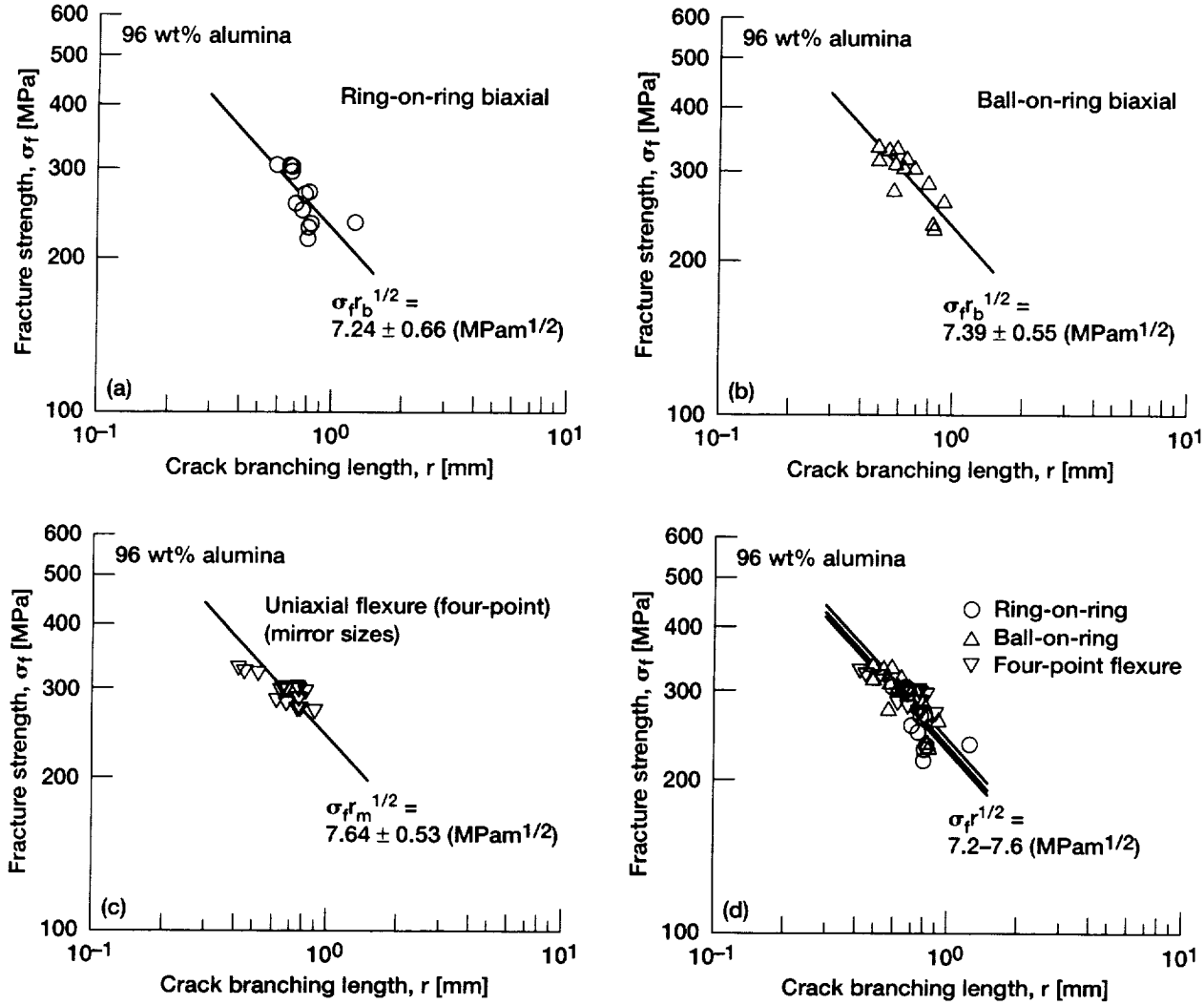

Figure 18.—Results of crack branching and fracture mirror size measurements for 96 wt% alumina: (a) ring-on-ring biaxial plate test specimens; (b) Ball-on-ring biaxial plate test specimens; (c) Four-point uniaxial flexure rectangular beam test specimens; (d) summary of all three cases.

1.1 to 3, has been reported among polycrystalline ceramics and glass [e.g., refs. 17 and 23 to 27). However, it should be noted that for glass the ratio of $A/K_{IC} \approx 3$ has been known as a unique material parameter regardless of flaw history such as loading, flaw types and environment (refs. 17, 26 and 27). The fact that the crack branching and fracture mirror constants determined from 96 wt % alumina are in reasonable agreement to each other is another but indirect indication of the valid strength measurements made in this test program.

PREDICTION

CARES/*LIFE* Design Code

A rigorous, accurate life prediction of a component from one specimen/loading configuration to another can be made using the NASA Glenn developed, CARES/*Life* public domain computer program. This can be achieved by determining statistical strength and SCG parameters in conjunction with results from finite element analysis of test specimens or structural components. Details regarding methodology of parameter estimation and component reliability are provided elsewhere (ref. 2) and are repeated here only briefly.

The CARES/*Life* time-dependent reliability analysis code, which uses the Batdorf multiaxial model (several other models are also incorporated in the code) (refs. 28 and 30), depends on self-similar (crack growth within the same plane) fatigue crack growth laws. For the power law, a generalized SCG formula, the same in principle as equation (2), is expressed as follows:

$$\frac{da(\Psi,t)}{dt} = A\,K_{Ieq}^{n}(\Psi,t) \tag{8}$$

where ψ represents a spatial location and orientation for the crack. K_{Ieq} is an equivalent mode I stress intensity factor

$$K_{Ieq}^{n}(\Psi,t) = \sigma_{Ieq}(\Psi,t)Y\sqrt{a(\Psi,t)} \tag{9}$$

where Y is a function of crack geometry, σ_{Ieq} is the equivalent mode I far field stress normal to a crack. From equations (8) and (9) it can be shown that for a given time interval, the equivalent transformed stress distribution $\sigma_{Ieq,0}(\Psi)$ at the beginning of that time interval $t = 0$ is related to the degraded strength $\sigma_{Ieq,f} = \sigma_{Ieq}(\psi,t_f)$ at the end of the time interval $t = t_f$ through the following equation:

$$\sigma_{Ieq,0}(\Psi) = \left[\frac{\int_0^{t_f}\sigma_{Ieq}^{n}(\Psi,t)dt}{B} + \sigma_{Ieq}^{n-2}\left(\Psi,t_f\right)\right]^{\frac{1}{(n-2)}} \tag{10}$$

$$B = \frac{2}{A\,Y^2 K_{IC}^{n-2}(n-2)} \tag{11}$$

The time-dependent reliability of a ceramic component can be computed assuming a crack density distribution, which is a function of the critical effective stress distribution. For surface analysis, the probability of survival, $P_{SS}(t_f)$, based on the Batdorf model (refs. 28 to 30) is

$$P_{SS}\left(t_f\right) = \exp\left[-\frac{\bar{k}_{BS}}{\pi}\int_A\int_0^{\pi}\left[\frac{\sigma_{Ieq,0}(\Psi)}{\sigma_{0S}}\right]^{m_S} d\alpha dA\right] \tag{12}$$

where $\bar{k}_{BS}$ is the normalized Batdorf crack density coefficient for surface flaws, $\sigma_{Ieq,0}(\Psi)$ is the transformed critical effective stress distribution at $t = 0$ as given in equation (10), σ_{0S} is the Weibull scale parameter for surface flaws, m_S is the Weibull modulus, and A denotes surface area. $\sigma_{Ieq,0}(\Psi)$ is dependent on the appropriate fracture criterion, crack shape, and time t_f.

The Batdorf method also depends on a mixed-mode fracture criterion and flaw shape. Using the criterion proposed by Shetty (ref. 31), an effective stress $\sigma_{Ieq}(\Psi,t)$ is expressed

$$\sigma_{Ieq}(\Psi,t) = \frac{1}{2}\left[\sigma_N(\Psi,t) + \sqrt{\sigma_N^2(\Psi,t) + 3.301\left(\frac{\tau(\Psi,t)}{\bar{C}}\right)^2}\right] \tag{13}$$

where σ_N is normal stress and τ is the shear stress on the flaw at (Ψ,t), and $\bar{C}$ is Shetty's (empirical) constant in mixed-mode fracture, called 'shear sensitivity parameter.' Shetty's constant $\bar{C}$ is empirical in that an appropriate value of $\bar{C}$ can be chosen to fit to a given set of data. Typical values of $\bar{C}$ range from 0.2 to 2.0.

The CARES/*Life* reliability analysis was performed to predict fatigue strength in both ring-on-ring biaxial flexure and ball-on-ring biaxial flexure, based on the SCG data determined in four-point uniaxial flexure. A similar work but at elevated temperature was done previously using the data generated from a silicon nitride at 1300 °C in four-point uniaxial flexure and ring-on-ring biaxial flexure (ref. 32). It was assumed here that failure was all associated with surface flaws, since test-specimen (tension) surface was a region most susceptible to slow crack growth because of its direct exposure to water, as also supported in part by fractographic analysis. The finite element meshes (quarter symmetry models) used to determine stress distributions of square plate test specimens subjected to ring-on-ring biaxial flexure and ball-on-ring biaxial flexure are shown in figure 19. The resulting stress distributions—normalized maximum principal stress—are depicted in figure 20. A state of biaxial stresses within both the loading ring in the ring-on-ring configuration and the loading contact-zone in the ball-on-ring configuration was evident. The analytical solutions, equations (3) and (5), were found to be in good agreement with the finite element analysis.

Based on the procedures described above together with the parameters estimated as well as with the stress distributions by finite element analysis, reliability predictions were made for the cases of ring-on-ring and ball-on-ring biaxial flexure. Their corresponding results are shown in figures 21 and 22, respectively for ring-on-ring and ball-on-ring biaxial flexure. A value of shear sensitivity parameter of $\overline{C} = 0.8$ was used for both predictions. A 95 percent confidence limit was also included in the figures. As can be seen from the figures, the predictions from the four-point uniaxial flexure data were in very reasonable agreement with the experimental data obtained from ring-on-ring and ball-on-ring biaxial flexure. This again indicates that the time-dependent effects of multiaxial stress state and the amount of material under stress can be accounted for using the time-dependent probabilistic design methodology as incorporated in the CARES/*Life* design code.

Analytical Method (PIA model)

The prediction of strength from one specimen/loading configuration to another will be made in this section based on a simple analytical, statistical model, called the principle of independent action (PIA) model (refs. 2 and 3). As for the CARES/*Life* prediction, failure was here assumed all associated with surface flaws, since test-specimen (tension) surface was a region most susceptible to slow crack growth because of its direct exposure to water. According to the PIA model, the (inert) strength of one test specimen (Specimen '1') having one specified surface area (or volume) can be related to that of another test specimen (Specimen '2') having another specified surface area (or volume) as follows:

$$\sigma_1 = \sigma_2 \left[\frac{A_{eff_2}}{A_{eff_1}} \right]^{\frac{1}{m}} \tag{14}$$

where the subscripts '1' and '2' denote any quantities associated with Specimens '1' and '2', and A_{eff} is the effective surface area, defined as follows

$$A_{eff} = \int_S \left(\frac{\sigma}{\sigma_o} \right)^m dA \tag{15}$$

where σ_o is the reference stress (or a maximum stress occurring in test specimen) and S is the surface area subjected to tensile stress (compressive stress treating as zero).

The effective surface areas for different specimen/loading configurations can be derived from equation (15) once the stress distributions throughout the test specimen are known. The following is a summary of the effective areas derived based on equation (15) for different specimen/loading configurations used in this work.

1. Rectangular beam test specimen in four-point uniaxial flexure:

$$A_{eff} = \frac{(L_i m + L_o)[B(m+1)+W]}{(m+1)^2} \tag{16}$$

where L_o and L_i are the outer and inner spans, respectively, B is the specimen width, and W is the specimen height.

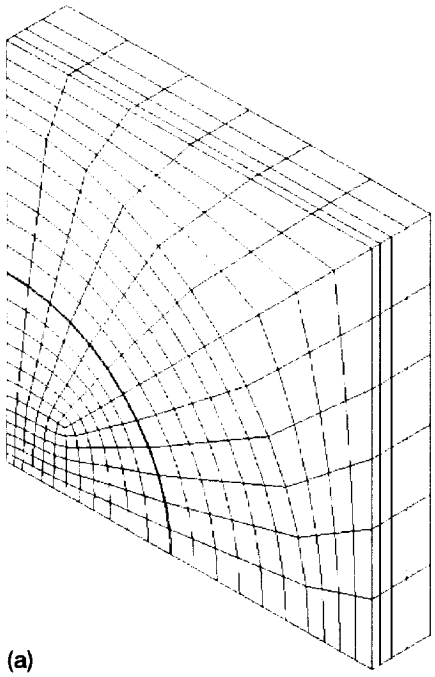

(a)

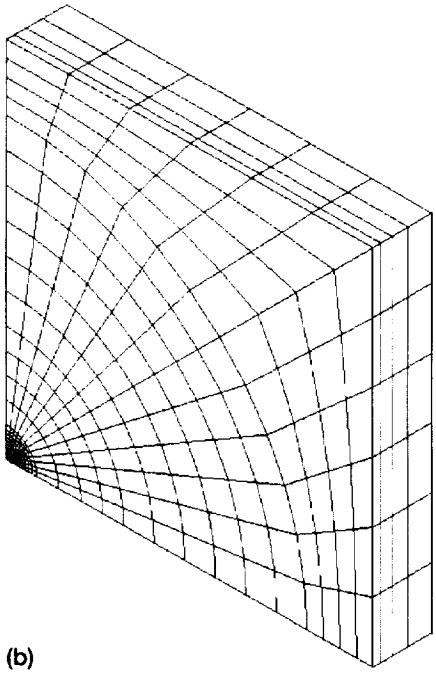

(b)

Figure 19.—Finite element meshes used for : (a) Square plate test specimen in ring-on-ring biaxial flexure; (b) Square plate test specimen in ball-on-ring biaxial flexure (quarter symmetry model).

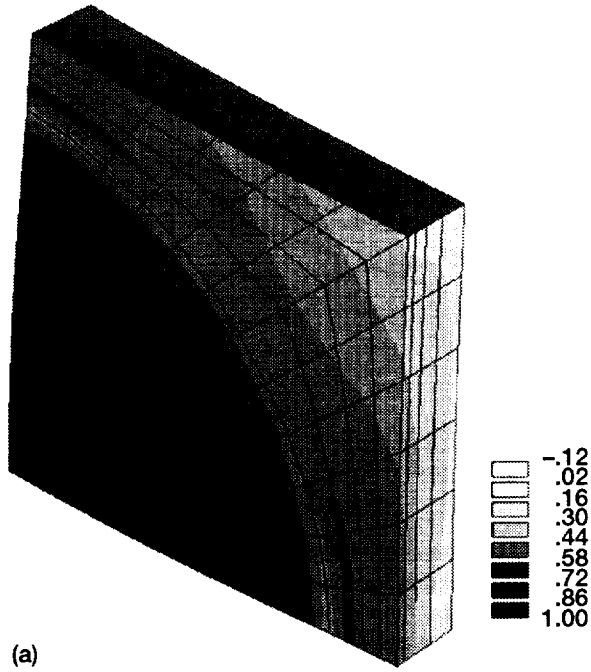

(a)

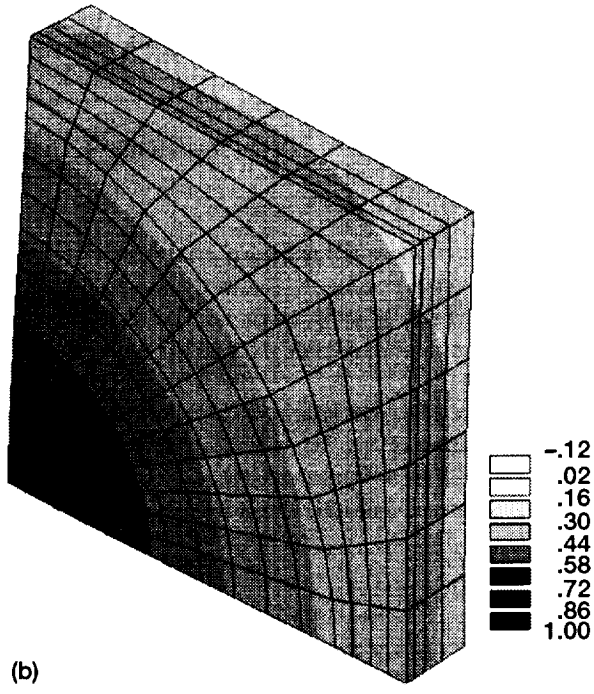

(b)

Figure 20.—Typical examples of (normalized maximum principle) stress distributions determined by finite element analysis for: (a) Square plate test specimen in ring-on-ring biaxial flexure; (b) Square plate test specimen in ball-on-ring biaxial flexure (quarter symmetry model).

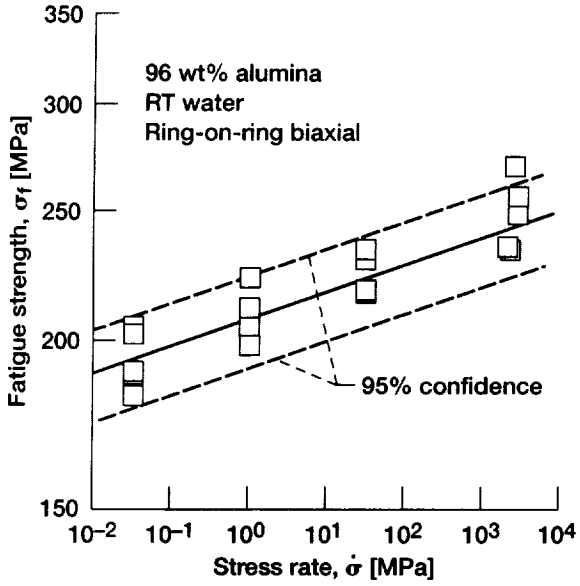

Figure 21.—Results of fatigue-strength prediction of 96 wt% alumina for the ring-on-ring biaxial tests specimens by the CARES/*Life* code based on the four-point uniaxial flexure data. The 95% confidence limit was included in the figure.

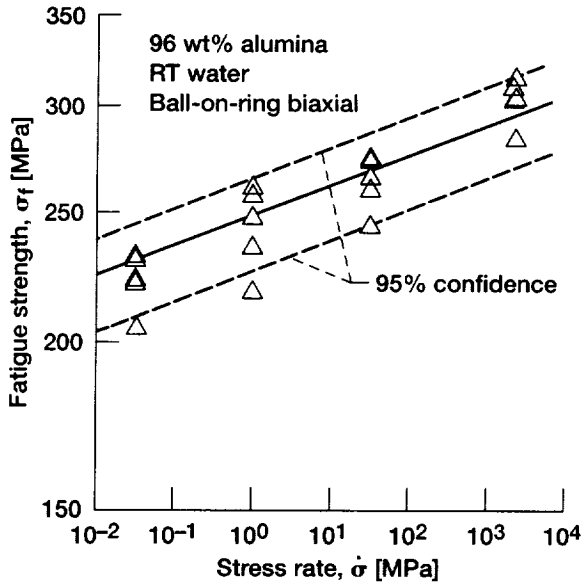

Figure 22.—Results of fatigue-strength prediction of 96 wt% alumina for the ball-on-ring biaxial tests specimens by the CARES/*Life* code based on the four-point uniaxial flexure data. The 95% confidence limit was included in the figure.

2. Square plate test specimen in ring-on-ring biaxial flexure:

$$A_{eff} = 2\pi b^2 + 2\pi \int_b^a \left[\left(\frac{\sigma_r}{\sigma_{\max}} \right)^m + \left(\frac{\sigma_t}{\sigma_{\max}} \right)^m \right] r\,dr \tag{17}$$

where σ_r and σ_t are radial and tangential stresses outside the loading-ring diameter, respectively, $\sigma_{\max}$ is the (maximum biaxial) stress occurring inside the loading-ring diameter, and r is radius in the polar coordinate system with origin of the center of a test specimen. The effective area can be estimated by numerical integration with the known equations of σ_r and σ_t outside the loading-ring diameter (ref. 12) together with $\sigma_{\max}$ expressed in equation (3).

3. Square plate test specimen in ball-on-ring biaxial flexure:

The equation of A_{eff} for the case of ball-on-ring biaxial flexure is the same as equation (17). However, σ_r and σ_t (ref. 12) are different from those for ring-on-ring biaxial flexure. The equation for $\sigma_{\max}$ is given in equation (5).

4. Dog-boned cylindrical test specimen in pure tension:

$$A_{eff} = \pi D L_g \tag{18}$$

where D is the test specimen diameter and L_g is the gage length.

5. Cylindrical beam test specimen in four-point uniaxial flexure:

$$A_{eff} = \frac{D(L_i m + L_o)}{2(m+1)} \int_0^{\pi} \sin^m \theta \, d\theta \tag{19}$$

where D is the test-specimen diameter, and L_o and L_i are the same as defined in equation (16). This equation can be solved only numerically since an analytical solution is not generally available because of its functional form. The analytical solution exists only for the integer number of m with a condition of $m < 3$.

With the effective area determined for a specific specimen/loading configuration using one of the above equations, a prediction of fatigue strength from one specimen/loading configuration to another can be made following the procedure given below. Equation (1) using equation (7) can be written as follows:

$$\sigma_f = \left[B(n+1)\sigma_i^{n-2}\right]^{\frac{1}{n+1}} \dot{\sigma}^{\frac{1}{n+1}} \tag{20}$$

Hence, for a given environment/material/flaw population system the fatigue strengths of Specimens '1' and '2' having different effective surface areas can be related from equations (14) and (20) with equation (1), as follows:

$$\sigma_{f_1} = \sigma_{f_2}\left[\frac{\sigma_{i_1}}{\sigma_{i_2}}\right]^{\frac{n-2}{n+1}} = D_2\left[\frac{\sigma_{i_1}}{\sigma_{i_2}}\right]^{\frac{n-2}{n+1}} \dot{\sigma}^{\frac{1}{n+1}} \tag{21}$$

or

$$\sigma_{f_1} = D_2\left[\frac{A_{eff_2}}{A_{eff_1}}\right]^{\frac{n-2}{m(n+1)}} \dot{\sigma}^{\frac{1}{n+1}} \tag{22}$$

Equation (16) with the appropriate A_{eff}'s and SCG parameters can be used to predict fatigue strength from one specimen/loading configuration to another with the assumption that the flaw population remains unchanged. The fatigue (n and D) and inert strength (m) data obtained from the four-point unaxial flexure test specimens were taken as a baseline reference for the prediction, which were $n = 47$, $\log D = 2.349$ and $m = 20.2$. The resulting prediction at a level of 50 percent reliability (without taking statistical aspect (e.g., confidence level, etc) into account) is presented in figure 23. As can be seen in the figure, the prediction for both ball-on-ring biaxial and ring-on-ring biaxial

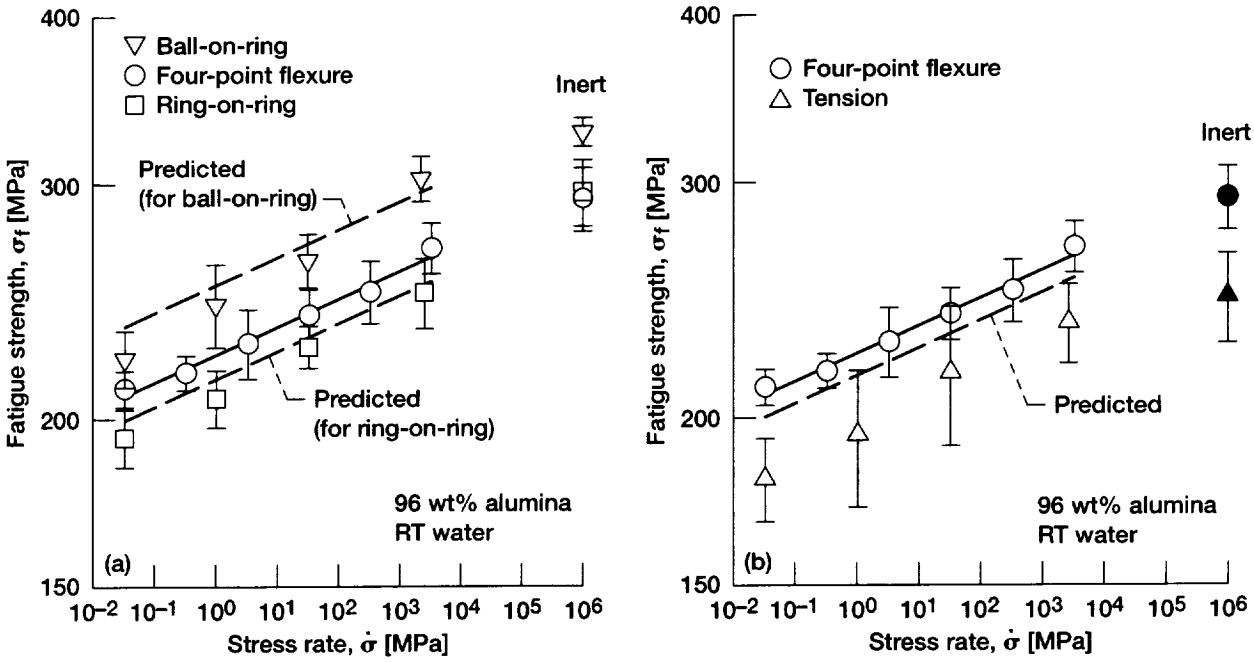

Figure 23.—Results of predictions of fatigue strength of 96 wt% alumina by the PIA method based on the four-point uniaxial flexure data. (a) Predicted for ring-on-ring biaxial and ball-on-ring biaxial flexure. (b) Predicted pure tension.

flexure was in good agreement with the actual data. By contrast, the prediction for tension was poor with the overall predicted strength being about 10 percent higher than the actual data.

As stated earlier, the as-received tensile test specimens showed chatter marks, undercuts and spiral machining marks on their gage sections, indicative of poor machining quality. As mentioned before, the tensile test specimens had to be polished with SiC papers and then annealed at 1200 °C for 1 hr. A plausible reason for such a significant discrepancy in fatigue-strength prediction (fig. 23(b)) was believed attributed to the difference in flaw population between the tensile test specimens and the four-point uniaxial flexure test specimens. To verify this hypothesis, a new test specimen configuration was made from the tensile test specimens such that some of the tensile test specimens (pin-hole, shoulder, or transition region broken specimens) were cut into uniform diameter, cylindrical rod test specimens with a length of about 20 mm (i.e., simply cutting off the upper and lower heads of each tensile test specimen). The test specimens were then annealed at 1200 °C for 1 hr in an attempt to have the specimens' surface conditions recovered to their original conditions prior to the previous tensile testing. This method has been proved appropriate for the test material and has been used customarily in this Lab. The test specimens, termed 'cylindrical rod test specimens,' were then subjected to constant stress-rate testing in room-temperature distilled water in four-point flexure with 9.617 mm-inner and 18.425 mm-outer spans. The electromechanical test frame was used in load control. Only two stress rates of 0.0333 and 33.33 MPa/s were employed, due to the limited number of test specimens available, with a total of 5 specimens at each stress rate.

Results of constant stress-rate testing for the cylindrical rod test specimens in four-point flexure are shown in figure 24. The resulting prediction based on the data for the rectangular flexure-beam test specimens is also shown in the figure. The tensile fatigue data and its related prediction were included for comparison. Surprisingly, contrast to the case for the tensile testing, agreement between the prediction and the actual data for the cylindrical rod test specimens was excellent. This implies that the flaw population of the cylindrical rod test specimens would have been very similar to those of the rectangular beam test specimens. Therefore, the hypothesis that the poor agreement between the prediction from uniaxial flexure (with rectangular beam) and the actual tensile data would be attributed to the difference in flaw population seems to be unjustified. Note again that all the test specimens used in this test

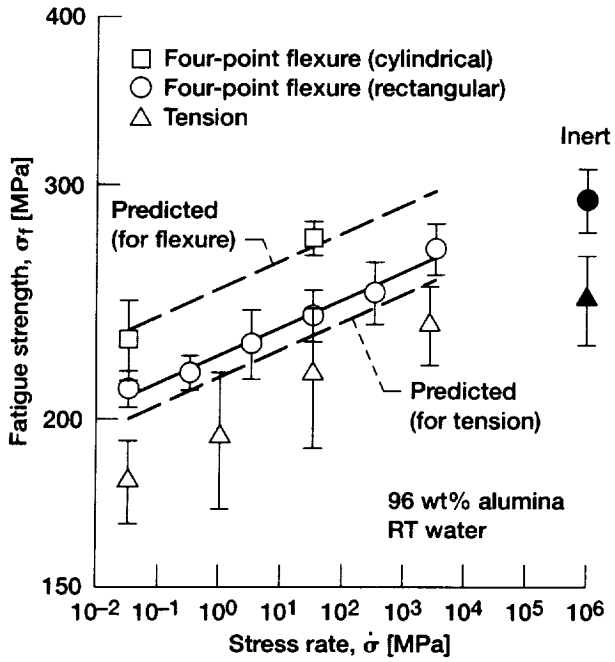

Figure 24.—Results of fatigue-strength prediction of 96 wt% alumina for the cylindrical rod uniaxial flexure test specimens (cut from the tensile test specimens) by the PIA method based on the four-point uniaxial flexure data. The original tensile data were included for comparison.

program were annealed with the same condition just prior to the individual testing, to ensure the consistent conditions of test-specimen surfaces. The exact reason for the inconsistent behavior exhibited by the tensile test specimens is not clear yet. Elaborate experimental work regarding this issue is needed to pinpoint a key aspect.

CONCLUSIONS

Constant stress-rate testing for 96 wt % alumina was performed in distilled water at room temperature using four different specimen/loading configurations such as four-point flexure, ring-on-ring biaxail flexure, ball on-ring biaxial flexure, and pure tension. The SCG parameter n for 96 wt % alumina was almost independent of specimen/loading configurations, either in four-point flexure, ring-on-ring biaxial, ball-on-ring biaxial flexure, or in pure tension, ranging from $n = 35$ to 47 with an average value of $n = 41.1 \pm 4.5$. This indicates that the SCG parameter n of 96 wt % alumina is a unique material constant for a given material/environment system. The prediction of fatigue-strength/reliability based on the four-point uniaxial flexure data using the CARES/*Life* design code as well as a PIA model was in good agreement with both the ring-on-ring biaxial and the ball-on-ring biaxial data. By contrast, a poor prediction (used by the PIA model) was observed for the dog-boned tensile test specimens, presumably due to different flaw population involved in tensile test specimens.

REFERENCES

1. S.R. Choi and J.A. Salem, "Free-Roller versus Fixed-Roller Fixtures in Flexure Testing of Advanced Ceramic Materials," Ceram. Eng. Sci. Proc., vol. 17, no. 3, 1996, pp. 69–77.
2. N.N. Nemeth, L.M. Powers, L.A. Janosik, and J.P. Gyekenyesi, "Time Dependent Reliability Analysis of Monolithic Ceramic Components using the CARES/*LIFE* Integrated Design Program," Life Prediction Methodologies and Data for Ceramic Materials, ASTM STP 1201, C.R. Brinkman and S.F. Duffy, eds., American Society for Testing and Materials, Philadelphia, 1994, pp. 390–408.
3. R.L. Barnett, C.L. Connors, P.C. Hermann, and J.R. Wingfield, "Fracture of Brittle Materials under Transient Mechanical and Thermal Loading," U.S. Air Force Flight Dynamics Laboratory, AFFDL-TR-66-220 (1967).
4. A.M. Freudenthal, "Statistical Approach to Brittle Fracture," Fracture, vol. 2: An Advanced Treatises, Mathematical Fundamentals, H. Liebowitz, ed., Academic Press, 1968, pp. 1–30.
5. S.R. Choi and J.A. Salem, "Dynamic, Static and Cyclic Fatigue of Alumina with Indentation-Induced Flaws," J. Mater. Sci. Lett., vol. 14, 1995, pp. 1286–1288.
6. A.G. Evans, "Slow Crack Growth in Brittle Materials under Dynamic Loading Conditions," Int. J. Fracture, vol. 10, 1974, pp. 251–159.
7. S.M. Wiederhorn, "Subcritical Crack Growth in Ceramics," Fracture Mechanics of Ceramics, vol. 2, R.C. Bradt, D.P.H. Hasselman, and F.F. Lange, eds., Plenum Press, New York, 1974, pp. 613–646.
8. S.R. Choi, J.A. Salem, and F.A. Holland, "Estimation of Slow Crack Growth Parameters for Constant Stress-Rate Test Data of Advanced Ceramics and Glass by Individual Data and Arithmetic Mean Methods," NASA TM–107369, Lewis Research Center, National Aeronautics and Space Administration, Cleveland, OH, 1997.
9. J.E. Ritter, "Engineering Design and Fatigue Failure of Brittle Materials," Fracture Mechanics of Ceramics, vol. 4, R.C. Bradt, D.P.H. Hasselman, and F.F. Lange, eds., Plenum Publishing Co., New York, 1978, pp. 667–686.
10. S.R. Choi, Standard Draft: "Standard Test Method for Determination of Slow Crack Growth Parameters of Advanced Ceramics by Constant Stress-Rate Flexural Testing at Ambient Temperature," C-28 Advanced Ceramics Committee, American Society for Testing and Materials, West Conshohocken, PA, 1997.
11. ASTM C1368-97, "Standard Test Method for Determination of Slow Crack Growth Parameters of Advanced Ceramics by Constant Stress-Rate Flexural Testing at Ambient Temperature," Annual Book of ASTM Standards, vol. 15.01, American Society for Testing and Materials, West Conshohocken, PA, 2000.
12. D.K. Shetty, A.R. Rosenfield, P. McGuire, G.K. Bansal, and W.H. Duckworth, "Biaxial Flexure Test for Ceramics," Ceram. Bull., vol. 59, no. 12, 1980, pp. 1193–1197.
13. F.F. Vitman and V.P. Pukh, "A Method for Determining the Strength of Sheet Glass," Zavodskaya Laboratoriya (Russia), vol. 29, no.7, 1963, pp. 863–867.

14. D.F. Carrol, S.M. Wiederhorn, and D.E. Roberts, "Technique for Tensile Creep Testing of Ceramics," J. Am. Ceram. Soc., vol. 72, 1989, pp. 1610–1614.
15. S.R. Choi, J.A. Salem, and J.L. Palko, "Comparison of Tension and Flexure to Determine Fatigue Life Prediction Parameters at Elevated Temperatures," Life Prediction Methodologies and Data for Ceramic Materials, ASTM STP 1201, C.R. Brinkman and S.F. Duffy, Eds., American Society for Testing and Materials, Philadelphia, 1994, pp. 98–111.
16. T. Ohji, "Towards Routine Tensile Testing," Int. J. High. Technol. Ceram., vol. 4, 1988, pp. 211–225.
17. J.J. Mecholsky, S.W. Freiman, and R.W. Rice, "Fracture Surface Analysis of Ceramics, J. Mater. Sci., vol. 11, 1976, pp. 1310–1319.
18. R.F. Cook, B.R. Lawn, and C.J. Fairbanks, "Microstructure-Strength Properties in Ceramics: II. Fatigue Relations," J. Am. Ceram. Soc., vol. 68, no. 11, 1985, pp. 616–623.
19. L-Y. Chao and D.K. Shetty, "Time-Dependent Strength Degradation and Reliability of an Alumina Ceramic Subjected to Biaxial Flexure," Life Prediction Methodologies and Data for Ceramic Materials, ASTM STP 1201, C.R. Brinkman and S.F. Duffy, Eds., American Society for Testing and Materials, Philadelphia, 1994, pp. 228–249.
20. K. Jakus, T. Service, and J.E. Ritter, "High-Temperature Fatigue Behavior of Polycrystalline Alumina," J. Am. Ceram. Soc., vol. 63, no. 1–2, 1980, pp. 4–7.
21. J.E. Ritter and J.N. Humenik, "Static and Dynamic Fatigue of Polycrystalline Alumina," J. Mater. Sci., vol. 14, 1979, pp. 626–632.
22. D.A. Krohn and D.P.H. Hasselman, "Static and Cyclic Fatigue Behavior of a Polycrystalline Alumina," J. Am. Ceram. Soc., vol. 55, no. 4, 1972, pp. 208–211.
23. D.K. Shetty, A.R. Rosenfield and W.H. Duckworth, "Crack Branching in Ceramic Disks Subjected to Biaxial Flexure," J. Am. Ceram. Soc., vol. 66, 1983, pp. C10–C12.
24. J.J. Mecholsky, S.W. Freiman, and R.W. Rice, "Fractographic Analysis of Ceramics, Fractography in Failure Analysis, ASTM STP 645, B.M. Strauss and W.H. Cullen, Eds., American Society for Testing and Materials, 1978, pp. 363–379.
25. S.R. Choi and J.P. Gyekenyesi, "Crack Branching and Fracture Mirror Data of Glasses and Advanced Ceramics," NASA/TM-1988–206536, National Aeronautics and Space Administration, Lewis Research Center, Cleveland, Ohio, 1998.
26. J.J. Mecholsky, R.W. Rice, and S.W. Freiman, "Prediction of Fracture Energy and Flaw Size in Glasses from Measurements of Mirror Size, "J. Am. Ceram. Soc., vol. 57, no. 10, 1974, pp. 440–443.
27. S.R. Choi and J.E. Ritter, "Fractographic Analysis of Fused Silica Optical Fibers with Subthreshold Indentation Flaws," Phys. Chem. Glasses, vol. 32, 1991, pp. 79–80.
28. S.B. Batdorf and J.G. Crose, "Statistical Theory for the Fracture of Brittle Structures Subjected to Nonuniform Polyaxial Stress," J. App. Mechanics, vol. 41, no. 2, 1974, pp. 459–464.
29. S.B. Batdorf and H.L. Heinisch, "Weakest Link Theory Reformulated for Arbitrary Fracture Criterion," J. Am. Cram. Soc., vol. 61, no. 7–8, 1978, pp. 355–358.
30. S.B. Batdorf, "Fundamentals of Statistical Theory of Fracture," Fracture Mechanics of Ceramics, vol. 3, Eds., R.C. Bradt, D.P.H. Hasselman, and F.F. Lange, Plenum Press, NY, 1978, pp. 1–30.
31. D.K. Shetty, "Mixed-Mode Fracture Criteria for Reliability Analysis and Design with Structural Ceramics," presented at the ASME Gas Turbine Conference and Exhibition, Anaheim, California, May 31–June 4, 1987, ASME paper No. 87-GT–70.
32. S.R. Choi, N.N. Noel, J.A. Salem, L.M. Power, and J.P. Gyekenyesi, "High Temperature Slow Crack Growth of Si_3N_4 Specimens Subjected to Uniaxial and Biaxial Dynamic Fatigue Loading Conditions," Ceram. Eng. Sci. Proc., vol. 16. no. 4, 1995, pp. 509–517.

REPORT DOCUMENTATION PAGE

Form Approved
OMB No. 0704-0188

1. AGENCY USE ONLY (*Leave blank*)	2. REPORT DATE	3. REPORT TYPE AND DATES COVERED
	July 2000	Technical Memorandum

4. TITLE AND SUBTITLE

Slow Crack Growth Behavior and Life/Reliability Analysis of 96 wt % Alumina at Ambient Temperature With Various Specimen/Loading Configurations

5. FUNDING NUMBERS

WU–505–23–1B-00

6. AUTHOR(S)

Sung R. Choi, Lynn M. Powers, and Noel N. Nemeth

7. PERFORMING ORGANIZATION NAME(S) AND ADDRESS(ES)

National Aeronautics and Space Administration
John H. Glenn Research Center at Lewis Field
Cleveland, Ohio 44135–3191

8. PERFORMING ORGANIZATION REPORT NUMBER

E–12325

9. SPONSORING/MONITORING AGENCY NAME(S) AND ADDRESS(ES)

National Aeronautics and Space Administration
Washington, DC 20546–0001

10. SPONSORING/MONITORING AGENCY REPORT NUMBER

NASA TM—2000-210206

11. SUPPLEMENTARY NOTES

Responsible person, Noel N. Nemeth, organization code 5920, (216) 433–3215.

12a. DISTRIBUTION/AVAILABILITY STATEMENT

Unclassified - Unlimited
Subject Categories: 07 and 39 Distribution: Nonstandard

This publication is available from the NASA Center for AeroSpace Information, (301) 621–0390.

12b. DISTRIBUTION CODE

13. ABSTRACT (*Maximum 200 words*)

Extensive constant stress-rate testing for 96 wt % alumina was conducted in room-temperature distilled water using four different specimen/loading configurations: rectangular beam test specimens under four-point uniaxial flexure, square plate test specimens in ring-on-ring biaxial flexure, square plate test specimens in ball-on-ring biaxial flexure, and dog-boned tensile test specimens in pure tension. The slow crack growth (SCG) parameter n was almost independent of specimen/loading configurations, in either four-point uniaxial flexure, ring-on-ring biaxial flexure, ball-on-ring biaxial flexure, or pure tension, ranging from $n = 35$ to 47 with an average value of $n = 41.1 \pm 4.5$. The prediction of fatigue strength/reliability based on the four-point uniaxial flexure data by using the CARES/*Life* design code as well as a simple PIA model was in good agreement with both the ring-on-ring biaxial and the ball-on-ring biaxial flexure data. A poor prediction using the PIA model was observed for the dog-boned tensile test specimens, presumably due to different flaw population involved in the tensile test specimens.

14. SUBJECT TERMS

Advanced ceramics; Alumina; Slow crack growth; Constant stress-rate testing; Dynamic fatigue; Life prediction

15. NUMBER OF PAGES

28

16. PRICE CODE

A03

17. SECURITY CLASSIFICATION OF REPORT	18. SECURITY CLASSIFICATION OF THIS PAGE	19. SECURITY CLASSIFICATION OF ABSTRACT	20. LIMITATION OF ABSTRACT
Unclassified	Unclassified	Unclassified	